Geologica Acta, Vol.7, Nº 3, September 2009, 389-397
DOI: 10.1344/105.000001444
Available online at www.geologica-acta.com

geologica acta

Chalcopyrite dissolution rate law from pH 1 to 3

P. ACERO* [1,2] **J. CAMA** [1] **C. AYORA** [1] **and M.P. ASTA** [1]

[1] **ICTJA and IDAEA Institute of Environmental Assessment and Water Research - CSIC**
c/ Jordi Girona 18-26, 08034 Barcelona, Spain

[2] **Petrology and Geochemistry Area, Earth Sciences Department, University of Zaragoza**
c/ Pedro Cerbuna 12, 50009 Zaragoza, Spain. E-mail: patricia.acero@unizar.es

*Corresponding author

ABSTRACT

Chalcopyrite dissolution kinetics in the pH range of 1 to 3 were studied by means of long-term flow-through experiments to obtain a dissolution rate law which can be coupled with reactive transport models to forecast Acid Rock Drainage.

In the range of conditions under study, the rate of chalcopyrite dissolution is only slightly dependent on hydrogen ion activity, increasing with decreasing pH. The steady-state dissolution rates obtained in the present study were combined with earlier results presented by Acero et al. (2007a) to obtain the following expression for chalcopyrite dissolution rate law:

$$R_{chalcopyrite} = 10^{-5.2\pm0.8}\, a_{H^+}{}^{0.16\pm0.04} e^{\frac{-31\pm4}{RT}}$$

where $R_{chalcopyrite}$ is the chalcopyrite dissolution rate (mol m^{-2} s^{-1}), a_{H^+} is the activity of hydrogen ion in solution, R is the gas constant (kJ mol^{-1} K^{-1}) and T is the temperature (K). This expression can applied through a wide range of environmental conditions similar to the ones found in systems affected by acid drainage.

In agreement with earlier chalcopyrite kinetic studies, iron was released to solution preferentially over copper and sulfur, compared with the stoichiometry of the pristine mineral. Consistently, XPS examination of the samples showed that reacted surfaces were enriched in sulfur and copper (relative to iron) compared with the initial, pristine chalcopyrite surface. However, this surface layer does not exert any passivating effect on chalcolpyrite dissolution and the kinetics of the overall process in the long term seems to be surface-controlled.

KEYWORDS | **Acid Mine Drainage. Kinetics. Flow-through. Sulfides.**

INTRODUCTION

Chalcopyrite ($CuFeS_2$) is the most abundant of the copper sulfides and its dissolution is the main agent responsible for the release of copper to groundwaters and surface run-off in environments affected by Acid Rock Drainage (ARD). Moreover, chalcopyrite is the main source for commercial copper production.

Because of this economical interest, most of the earlier works on chalcopyrite dissolution have focused on the use of different leaching media to improve the copper recovery (Munoz et al., 1979; Dutrizac, 1981; Çolak et al., 1987; Devi et al., 2000; Hiroyoshi et al., 2000, 2001; Adebayo et al., 2003; Antonijevic et al., 2004; Aydogan et al., 2006). Owing to their application to hydrometallurgy, the chemistry and temperature range assessed in these earlier studies are generally far from ARD and other weathering conditions.

One of the main drawbacks encountered during the process of copper recovery is related to the fact that chalcopyrite dissolves generally non-congruently, forming an iron-deficient surface structure which, in turn, is richer in sulfur than the pristine chalcopyrite surface (Dutrizac, 1990; Hackl et al., 1995; Fairthorne et al., 1997). Therefore, there have been an increasing number of studies focused on the evolution of chalcopyrite surface during dissolution (Parker et al., 1981; Buckley and Woods, 1984; Biegler and Horne, 1985; Hackl et al., 1995; Fairthorne et al., 1997; Lu et al., 2000; Klauber et al., 2001; Mikhlin et al., 2004; Harmer et al., 2006; Rosso and Vaughan, 2006 and references therein).

On the other hand, the works focused on the chalcopyrite dissolution kinetics in conditions analogous to ARD are much scarcer. The pioneer kinetic studies by Scharer et al. (1994) and Rimstidt et al. (1994) provided very valuable data on the initial rate of chalcopyrite dissolution at acidic pH (2-3). In the paper by Rimstidt et al. (1994) a rate law for chalcopyrite dissolution in the presence of Fe (III) was proposed. More recent studies have obtained chalcopyrite steady-state dissolution rates based on the copper release from pyritic tailings during flow-through experiments (Domènech et al., 2002; Salmon and Malmström, 2006). Finally, the chalcopyrite steady-state dissolution rates at pH 3, at temperatures from 25 to 70ºC and at dissolved oxygen concentrations between 8.7 and 0.2 mg L^{-1} were recently obtained by Acero et al. (2007a), which showed that chalcopyrite dissolution rates were independent of the availability of dissolved oxygen and proposed an overall surface-controlled dissolution reaction under those conditions.

Although these studies have shed light on the chalcopyrite dissolution kinetics, their results do not cover the common range of environmental conditions present during ARD. This study is aimed at bridging a part of this gap by proposing a dissolution rate law for chalcopyrite dissolution under a wide range of acidic conditions similar to those encountered in ARD systems. This will contribute to the improvement of geochemical and reactive transport models on the evolution of chalcopyrite in mining and natural environments, which is crucial for the prediction and remediation of ARD impact on the environment.

With this aim, the chalcopyrite steady-state dissolution rates at pH from 1 to 3 were obtained by means of stirred and non-stirred flow-through experiments. These dissolution rates were then combined with the results obtained by Acero et al. (2007a) by using the same experimental approach and lumped in a single rate law that can be easily incorporated into the kinetic databases of geochemical and reactive transport codes. Furthermore, the chalcopyrite pristine and reacted surfaces were examined by Scanning Electron Microscopy (SEM) and X-ray Photoelectron Spectroscopy (XPS) in order to better understand the interactions between the mineral surface and acidic solutions during dissolution.

MATERIALS AND METHODS

Sample characterization

The chalcopyrite sample used in this study is from El Molar (Catalonian Coastal Range, Spain). X-ray diffraction (XRD) performed on thoroughly crushed samples of the raw chalcopyrite showed no evidence of the presence of any other mineral phase. Microprobe analyses in multiple points confirmed the high purity of the sample (Table 1). Mineral samples were ground in agate mortar and sieved to obtain the fraction with particle size between 10 and 100 μm. The specific surface area of the ground raw sample was determined to be 0.71±0.1 m^2g^{-1} by the BET method (Brunauer et al., 1938) using 5-point N_2 adsorption isotherms. No attempt was made to remove fine particles (smaller than 1 μm) adhered to the initial surfaces given that the powders resulting from usual milling operations contain microparticles attached onto the grains. In some of the earlier dissolution studies, a treatment to remove microparticles (annealing, washing with water or ethanol, differential settling, etc.) was applied and, in some cases, a very narrow range of particle sizes was selected in order to reduce the variability of the samples. However, one advantage to using long-term flow-through experiments is that it is not necessary to pre-treat the samples in order to obtain steady-state dissolution rates since the possible effect that the particle size might exert is corrected by normalizing the rates using the final specific surface area.

XPS surface examination of the initial and reacted powdered samples, mounted on carbon conducive tabs, was carried out with a Physical Electronics (PHI) 5500 spectrometer using a monochromatic X-ray source (with an Al Kα line of 1486.6 eV energy and 350 W) placed perpendicular to the analyzer axis and calibrated using the

TABLE 1 | **Results (wt.% and at. %) of the microprobe analyses of chalcopyrite used in the experiments.**

Element	S	Fe	Cu	Zn	Pb
wt. %	35.25	30.20	34.39	0.04	0.13
at. %	50.37	24.78	24.80	0.02	0.03

3d5/2 line of Ag with a width of 0.8 eV and a binding energy of 368.3 eV. All these measurements were made in an ultra high vacuum (UHV) chamber (pressure between $6.6 \cdot 10^{-11}$ and $6.6 \cdot 10^{-12}$ atm). The analyser pass energy was 23 eV. An electron flood gun at low energies (below 25 eV) was used for charge compensation. Comparison of the relative positions of the different peaks in all the studied spectra indicated that charge shifting could be considered uniform. Spectra are shown as raw data corrected for the peak shifting due to charge by adjusting the C1s peak (corresponding to adventitious carbon) to a binding energy of 284.6 eV. Due to the lack of sample cooling while acquiring the measurements, loss of potentially present elemental sulfur could occur. Therefore, even if the presence of elemental sulfur was not confirmed, it is considered as a possibility in the discussion below.

Atomic concentrations of copper, iron and sulfur were determined from the XPS peak areas divided by atomic sensitivity factors subsequent to Shirley background substraction. Bulk-like spectra for the initial sample were obtained by using argon sputtering to remove any surface oxidation phase (Todd et al., 2003). A deconvolution of the spectra into different components was carried out. Each spectrum was fitted by means of an iterative least-squares procedure with Gaussian bands. The proportion of each surface species was then determined as a function of the areas covered by each band. However, a systematical quantification of the different sulfur and iron species present in the samples is not presented here because of the low signal-to-noise ratio in most of the XPS spectra for these peaks. Only the approximate position of the observed sulfur species will be described below.

Solutions

Input solutions of desired pH were prepared with analytical reagent grade hydrochloric or sulfuric acid and with distilled, double deionized water (18.2 MΩ· cm). A Crison meter and combined glass electrode with temperature compensation was used to measure pH and was calibrated regularly with 2 and 7 standard buffer solutions. Input and output pH were the same (within ±0.05 pH units of error). When possible, redox potential was measured by an Orion combination Pt/Ag-AgCl redox electrode. The measurements were referenced to the Standard Hydrogen Electrode (SHE). Reliable redox potential measurements could not systematically be obtained because of considerable drifting in the recorded values with time. This drifting can be explained by the presence of $H_2S(g)$, by the low concentrations of aqueous species in the target solutions (in most cases less than 10^{-5} mol L^{-1}) or even by the absence of a clearly dominant redox couple (Nordstrom, 2000). When the redox potential could be measured, it was always higher than 0.3 V.

The concentrations of dissolved oxygen were determined by a Hanna portable meter with compensation of temperature, salinity and altitude with an accuracy of ± 0.45 mg L^{-1}. Total iron, copper and sulfur concentrations in the solutions were determined by Inductively Coupled Plasma Atomic Emission Spectrometry (ICP-AES) using a Thermo Jarrel-Ash instrument with CID detector. Calibration with sets of standards was performed and the regression coefficient exceeded 0.999. Three laboratory standards were analyzed with every 10 samples to check for accuracy and the error was estimated to be below 3%. The detection limits for Fe, Cu and S were determined to be $1.8 \cdot 10^{-7}$, $1.6 \cdot 10^{-7}$ and $3.5 \cdot 10^{-6}$ mol L^{-1}, respectively. Error associated with ICP-AES measurement was estimated to be around 3%.

Flow-through experiments

The experimental setup used in the experiments has been described elsewhere (Acero et al., 2007a). Experiments were carried out using stirred (experiments with names beginning with Ccp) and non-stirred (experiments with names beginning with NS-Ccp) flow-through Lexan reactors with a reaction chamber volume of 40 mL in which the powdered sample and the stirrer were placed together. Reactors were immersed in thermostatized water baths to keep the temperature at 25 (± 1) ºC. Dissolved oxygen concentration in the input solutions was set to 8.7 mg L^{-1}. This was ensured by purging the input solution with a gas mixture with 20.5% O_2 and checking the dissolved oxygen concentration before pumping the input solution into the reactors.

Steady-state conditions were considered to be attained when differences in the metal concentration of the output solution were within ± 10% for at least 200 hours and four consecutive leachate samples. After the experiments, the reacted samples were collected, rinsed with double-distilled water, dried at room temperature and stored in closed microvials until examination by Scanning Electron

Microscopy (SEM), X-Ray Photoelectron Spectroscopy (XPS) and determination of BET surface area.

Calculation of dissolution rates

In a flow-through reactor, the steady-state dissolution rate is calculated according to the following simple mass-balance equation

$$r = \frac{q(c_i - c_i^o)}{A\nu_i} \quad (1)$$

where q is the flow rate of the solution through the reactor, ν_i is the stoichiometric coefficient of the i element in the studied material and A is the total surface area of the mineral sample in area units. The notations c_i and c_i^o represent the out-and in-flowing concentrations of the i element, respectively.

The error associated with the dissolution rates was calculated by the Gaussian error propagation method (Barrante, 1974) to be around 16% and is dominated by the uncertainty of BET surface area measurements (±15%).

RESULTS AND DISCUSSION

The steady-state results of the flow-through experiments are presented in Table 2. Most of the experiments ran for 800 to 1800 h, and steady state was generally attained after 500 to 1200 h from the beginning of the experiment and lasted for more than 200 h. Calculated total dissolved mass of chalcopyrite throughout the experiments was in all cases less than 4% of the initial mass of the sample.

Copper and iron concentrations in the output solutions were highest at the start of the experiments, decreasing thereafter until steady state was attained (Fig. 1). Initially high concentrations were probably due to the dissolution of the external, altered layers of the ground minerals and/or to the existence of microparticles.

Output sulfur concentrations were always below the detection limit and the typical $H_2S_{(g)}$ odour was identified when collecting the output solutions in some of the experiments (especially at pH 1). Sulfur deficit in solution was also found in the earlier work on chalcopyrite dissolution by Acero et al. (2007a) and has also been described in studies on the dissolution of other sulfide minerals, such as pyrite (Domènech et al., 2002), pyrrhotite (Janzen et al., 2000), sphalerite (Lochmann and Pedlik, 1995; Weisener et al., 2003, 2004; Acero et al., 2007b) or galena (De Giudici and Zuddas, 2001; Cama and Acero, 2005; Cama et al., 2005; Acero et al., 2007c).

With regard to output copper concentrations, they were always lower than output iron concentrations (Table 2). The non-stoichiometry Cu:Fe:S in solution has also been previously reported (Hackl et al., 1995; Fairthorne et al., 1997; Holliday and Richmond, 1990; Lu et al. 2000; Devi et al., 2000; Antonijevic and Bogdanovic, 2004; Acero et al., 2007a). Only in the experiments carried out at pH 1 (Ccp-1A, Ccp-1B and NS-Ccp-1) is the stoichiometry Cu:Fe similar to the proportion for these elements in the bulk chalcopyrite (Table 2). Since chalcopyrite dissolved non-congruently, the amount of dissolved chalcopyrite was assessed by the amount of dissolved iron, and dissolution rates were normalized using the steady-state mass and the BET surface area of the reacted sample.

The solution saturation state was estimated on the assumption that sulfur was released congruently from chalcopyrite. According to calculations run with the

TABLE 2 | **Experimental conditions, steady-state values and chalcopyrite dissolution rates obtained. The initial BET area of all the experiments is 0.71 $m^2\ g^{-1}$.**

Experiment	Acid type	flow rate (mL min^{-1})	pH	Fe	Cu	S	Fe/Cu	mass s.s. (g)	final BET area ($m^2\ g^{-1}$)	rate Fe	log (rate Fe)
				(mol L^{-1})						(mol $m^{-2}\ s^{-1}$)	
Ccp-3A	HCl	0.040	3.0	$3.2{\cdot}10^{-6}$	$1.5{\cdot}10^{-6}$	*b.d.l.*	2.1	0.81	0.39	$6.8{\cdot}10^{-12}$	-11.2
Ccp-2	HCl	0.038	2.0	$8.8{\cdot}10^{-6}$	$2.8{\cdot}10^{-6}$	*b.d.l.*	3.2	0.80	0.45	$1.6{\cdot}10^{-11}$	-10.8
Ccp-1A	HCl	0.045	1.0	$8.1{\cdot}10^{-6}$	$6.1{\cdot}10^{-6}$	*b.d.l.*	1.3	0.81	0.40	$1.9{\cdot}10^{-11}$	-10.7
Ccp-1B	H_2SO_4	0,040	1.0	$6.3{\cdot}10^{-6}$	$5.2{\cdot}10^{-6}$	*n.d.*	1.2	0.79	0.31	$1.7{\cdot}10^{-11}$	-10.8
Ccp-3B	H_2SO_4	0.035	3.0	$4.7{\cdot}10^{-6}$	$1.5{\cdot}10^{-6}$	*n.d.*	3.2	0.81	0.36	$9.3{\cdot}10^{-12}$	-11.0
NS-Ccp-3	HCl	0.031	3.0	$2.6{\cdot}10^{-6}$	$1.2{\cdot}10^{-6}$	*b.d.l.*	2.1	0.57	0.25	$9.4{\cdot}10^{-12}$	-11.0
NS-Ccp-2	HCl	0.029	2.0	$7.5{\cdot}10^{-6}$	$2.5{\cdot}10^{-6}$	*b.d.l.*	3.0	0.60	0.43	$1.4{\cdot}10^{-11}$	-10.9
Ns-Ccp-1	HCl	0.035	1.0	$5.3{\cdot}10^{-6}$	$4.6{\cdot}10^{-6}$	*b.d.l.*	1.2	0.59	0.35	$1.5{\cdot}10^{-11}$	-10.8

s.s. = steady state

b.d.l. = below detection limit (3.5 10^{-6} mol L-1 for S, $1.8{\cdot}10^{-7}$ mol L^{-1} for Fe and $1.6{\cdot}10^{-7}$ mol L^{-1} for Cu)

n.d. = not determined (dissolved sulfur in experiments carried out in sulfuric acid)

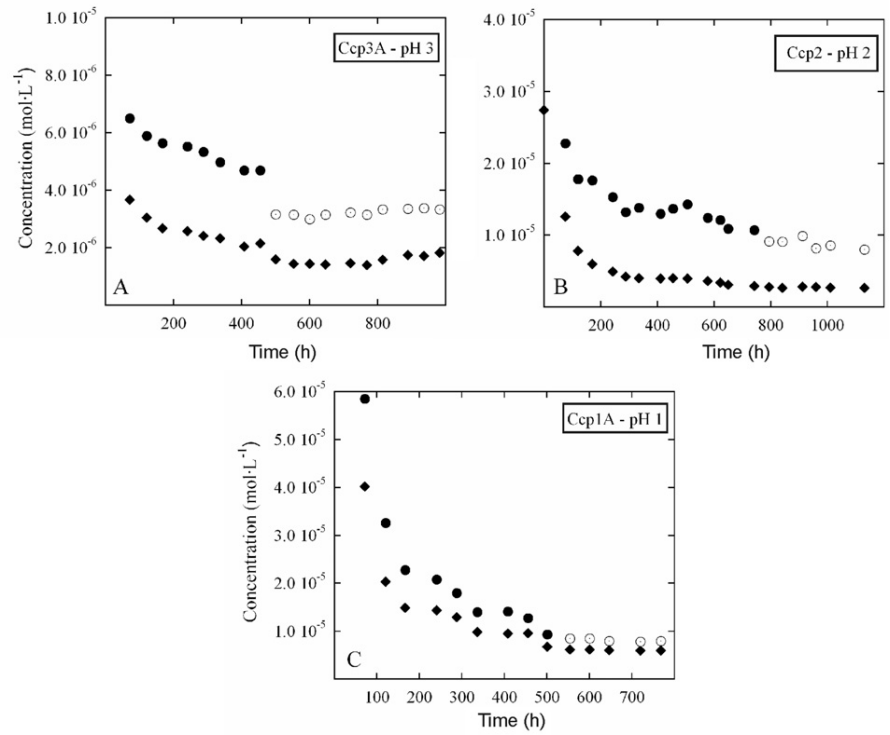

FIGURE 1 | **Variation in the concentrations of copper (rhombi) and iron (circles) vs. time in three of the experiments carried out at pH 3, 2 and 1 (A, B and C, respectively). Open symbols denote values of iron concentrations used to calculate average steady state. Initial concentrations for the experiments Ccp3A and Ccp1A are not depicted for the sake of significance of the vertical scale.**

PHREEQC code (Parkhusrt, 1995) using the lowest measured redox potential, all output solutions were very undersaturated with respect to chalcopyrite or to any other possible sulfide or sulfate phase.

The results obtained by the XPS examination of the samples before and after the experiments are summarized in Table 3. Almost all reacted samples displayed sulfur enrichment when compared with the initial unreacted surface. Assuming that the initial bulk sample was perfectly stoichiometric (ratio Cu:Fe:S equal to 1:1:2), in line with the microprobe analysis (Table 1), all reacted samples also showed enrichment in copper relative to iron after leaching. This observation is consistent with the enrichment in iron relative to copper observed in the solution (Table 2). Moreover, this feature has also been reported in earlier XPS studies on chalcopyrite dissolution (Price and Warren, 1986; Hackl et al., 1995; Fairthorne et al., 1997; Mikhlin et al., 2004).

The low signal-to-noise ratio in some of the XPS spectra in the region of both the S2s and the S2p peaks made a systematic quantification of the different sulfur species present in the samples impossible. However, four sulfur species can be identified in the S2p peak of all the samples, at binding energies (BE) of 161.4-161.8 eV, 162.9-163.3 eV, 164.4-164.9 eV and 168.2-169.0 eV for the S2p3/2 peak. Based on the BE values reported in earlier studies (Buckley and Woods, 1984; Fairthorne et al., 1997; Farquhar et al., 2003; Mikhlin et al., 2004), the lowest BE value was identified as S^{2-} (161.2-161.7 eV) and the highest (168.2-169.0 eV) was attributed to SO_4^{2-}. The species identified at middle energies were attributed to either polysulfides or elemental sulfur. The main species in all the spectra seems to be S^{2-}. In the light of S2p peak analyses, only minor amounts (possibly less than 15%) of surface sulfate were present in the reacted

TABLE 3 | **Surface stoichiometry obtained by the X-ray Photoelectron Spectroscopy (XPS) determinations on the initial and reacted chalcopyrite samples.**

Sample	S	Fe	Cu	S: (Cu+Fe)	Cu:Fe
	(at. %)[1]				
Initial $CuFeS_2$	50	25	25	1.0	1.0
Ccp-3A	76	9	16	3.1	1.7
Ccp-2	65	14	21	1.9	1.4
Ccp-1A	48	23	29	0.9	1.3
Ccp-1B	72	12	16	2.6	1.4
Ccp-3B	72	12	16	2.6	1.2

[1] *normalizing out other elements (oxygen and adventitious carbon)*

samples. The presence of elemental sulfur on the surfaces could not be confirmed nor discarded by this technique, due to the technical limitations of the equipment used in the acquisition of the spectra. However, examination of the samples by SEM (Fig. 2) showed no evidence of the presence of precipitates on the chalcopyrite reacted grains, even though they have been observed on chalcopyrite surfaces by other authors (Lu et al., 2000) under different experimental conditions but using the same technique.

The poor quality of the signal in the Fe2p region of the reacted chalcopyrite surfaces made the XPS identification and quantification of the iron surface species impossible. This is a common drawback in most earlier XPS studies focused on chalcopyrite (see e.g. Klauber et al., 2001). Regarding the Cu2p3/2 peak, the main species identified in all the reacted samples was found at BE of 931.3-931.8 eV, accounting for more than 70% of the total surface Cu in all cases. This peak was the only one to be positively identified in the initial bulk sample, and it was attributed to cuprous ions (Farquhar et al., 2003; Klauber, 2003). The contribution of the cupric component, identified at 932.9-933.7 eV (Klauber, 2003) is minor in all cases (less than 30%).

Significance of steady-state dissolution rates for chalcopyrite

As discussed in the previous section, chalcopyrite dissolution is not congruent and leads to the formation of a surface layer enriched in sulphur and copper compared with the pristine surface under the experimental conditions described in this paper. However, it is important to note that the surface dissolution products do not seem to be passivating chalcopyrite in the presence of either chloride or sulfate ions. If a passivating layer blocking the access of reactants and products were being created by dissolution, durable steady states, as depicted in Fig. 1, would never be attained. One possible explanation is that the surface layer is porous and not uniform, in line with earlier results (Palmer et al., 1981; Farquhar et al., 2003; Velásquez et al., 2005; Aydogan et al., 2006).

The obtained rates for chalcopyrite dissolution are in good agreement with the only two earlier works presenting results from long-term experiments (Table 4). The fact that our rates are slightly slower than the ones proposed by Domènech et al. (2002) and Salmon and Malmström (2006) can be attributed to differences in the initial material used in the experiments. These two studies based their calculations on the amount of released copper from tailing samples (not from pure chalcopyrite samples) with less than 1% chalcopyrite and containing other Cu-bearing phases, namely tetrahedrite-tenantite in the case of the Aznalcollar sample (Almodovar et al., 1998) and covellite in the case of Kristinesberg (Salmon and Malmström, 2006). If a part of the released copper corresponds to the dissolution of those accompanying Cu-phases and not to chalcopyrite dissolution, the observed copper release may not fully correspond to chalcopyrite dissolution and it may have led to an overestimation of the rates presented by Domènech et al. (2002) and Salmon and Malmström (2006).

As explained above, the dissolution rates obtained in the experiments carried out with hydrochloric acid were the same, within error, as the rates obtained at the same pH by using sulfuric acid. Although the acid type can produce differences in the initial leaching behavior of chalcopyrite, as reported previously by Lu et al. (2000), the steady-state results (dissolution rates, durability of steady state, copper/iron ratios in solution and in the reacted surfaces) seemed to be independent of the type of leachant under the experimental conditions presented

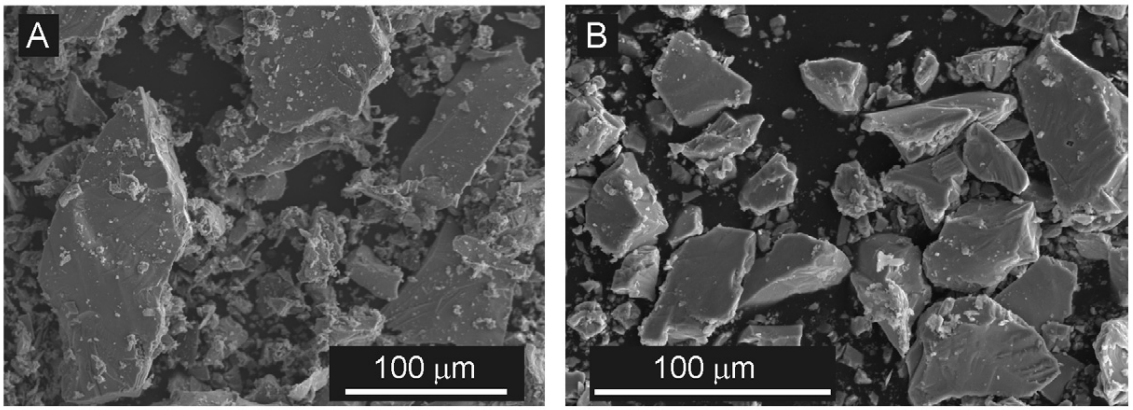

FIGURE 2 | **SEM images of the samples used in the experiments. A) Freshly ground and sieved chalcopyrite before the experiments, and B) Chalcopyrite grains after the experiment Ccp3A (pH 3).**

TABLE 4 | **Comparison of chalcopyrite dissolution rates in this study and in earlier long-term dissolution studies.**

Reference	Experiment type	Solution type / pH	T (ºC)	rate (mol m^{-2} s^{-1})
Salmon and Malmström (2006)	Batch reactor	HNO_3-H_2SO_4 / pH 2 (approx.)	23	$4.05 \pm 1.65 \cdot 10^{-10}$
Domènech *et al.* (2002)	Flow through	HCl / pH 3.05	25	$8 \pm 2 \cdot 10^{-11}$
This study	Flow through	HCl / pH 2	25	$1.5 \pm 0.2 \cdot 10^{-11}$
		HCl / pH 3	25	$8.4 \pm 1.2 \cdot 10^{-12}$

in this paper. Therefore, the results obtained in this study are applicable for the prediction of chalcopyrite behavior in ARD systems, in which the main anionic species is sulfate.

Effect of pH on dissolution rates and dissolution rate law

The variation of the chalcopyrite dissolution rate with pH at 25ºC and 8.7 mg L^{-1} DO is shown in Fig. 3. The dissolution rate of chalcopyrite slightly increased when pH decreased, in line with earlier results (Antonijevic and Bogdanovich, 2004). Calculation of the reaction order of chalcopyrite dissolution, with respect to a_{H^+} from the slope of the line of the logarithm of the rates vs. pH (Fig. 3), yielded a value of 0.16 ± 0.04.

In the earlier work of Acero et al. (2007a), the dissolution rates obtained at pH 3 under different conditions of dissolved oxygen availability at 25, 50 and 70ºC were combined to obtain the apparent activation energy associated with the overall dissolution reaction. Since the methodology in both studies is essentially identical, the dissolution rates obtained in this work, within the pH range from 1 to 3, can be combined with the results of Acero et al. (2007a). Thus, both sets of dissolution rates can be lumped into a single dissolution rate law by multiple linear regression. In the absence of other catalysts or inhibitors and under far-from-equilibrium conditions (Lasaga et al., 1994), the chalcopyrite dissolution rate between pH 1 and 3 and within the temperature range from 25 to 70ºC can therefore be expressed as:

$$R_{chalcopyrite} = 10^{-5.2 \pm 0.8} \, a_{H^+}{}^{0.16 \pm 0.04} e^{\frac{-31 \pm 4}{RT}} \quad (2)$$

where $R_{chalcopyrite}$ is the chalcopyrite dissolution rate (mol m^{-2} s^{-1}), a_{H^+} is the activity of hydrogen ion in solution, R is the gas constant (kJ mol^{-1} K^{-1}) and T is the temperature (K). The value of 31±4 kJ mol^{-1} which appears in the rate law represents the apparent activation energy of the overall dissolution reaction according to the experimental results presented by Acero et al. (2007a). As already explained by these authors, this value of the activation energy is consistent whith a surface-controlled dissolution reaction.

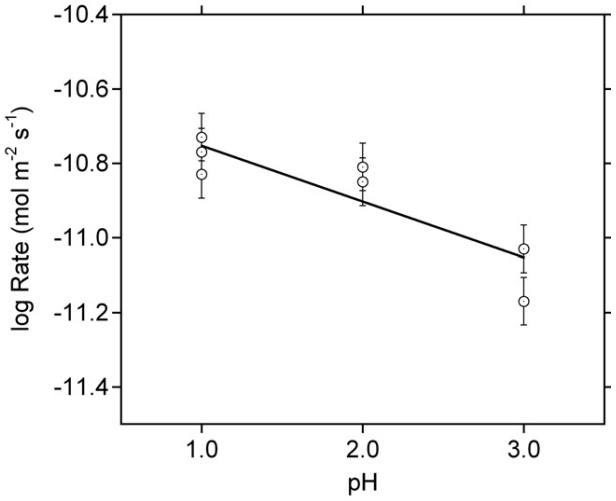

FIGURE 3 | **Chalcopyrite dissolution rate dependence on pH. The reaction order with respect to the H^+ activity is given by the slope of the plot (0.16 ± 0.04).**

This dissolution rate expression can easily be incorporated into the kinetic databases of the geochemical and reactive transport modelling codes, allowing a better prediction of the chalcolpyrite behavior and copper release in acid environments, such as in the systems affected by ARD.

CONCLUSIONS

Chalcopyrite dissolution rates at pH from 1 to 3 have been studied for the first time in long-term dissolution experiments. The steady-state dissolution rates of chalcopyrite are only slightly dependent on hydrogen ion activity, increasing with decreasing pH within the studied

range. Chalcopyrite dissolves incongruently, preferentially releasing iron over copper to solution. Consistently, its dissolution produces a surface layer enriched in copper and sulfur compared with the pristine mineral surface. However, this surface layer of elemental sulfur, sulfides and/or polysulfides does not seem to exert any passivating effect on chalcopyrite dissolution.

The environmental conditions addressed in this paper are very similar to the ones usually present in Acid Rock Drainage and, therefore, the obtained dissolution rates will be applicable to the prediction of the chalcopyrite long-term dissolution behavior in environments undergoing acid drainage. Moreover, the combination of the experimental results from this work with the rates obtained in the earlier dissolution study by Acero et al. (2007a), that showed that the chalcopyrite dissolution rate was not affected by the availability of dissolved oxygen under similar environmental conditions to the ones studied in this work, has allowed formulation of a dissolution rate law which can be used in geochemical and reactive transport calculations.

ACKNOWLEDGEMENTS

This work was funded by the Research and Development Contracts CTM2006-28151-E/TECNO and CTM2007-66724-C02-01/TECNO. Patricia Acero was also supported by a grant from the Spanish Government. We gratefully acknowledge the fruitful discussions with Araceli Garrido and Volker Metz and the analytical assistance of Javier Pérez, Rafael Bartrolí, Mercè Cabanes, Silvia Martínez and Josep Elvira from the Institute of Earth Sciences "Jaume Almera"-CSIC, and Lorenzo Calvo, Joaquim Portillo and Joan Gámez from the SCT of the University of Barcelona. The thorough reviews of Dr. Javier Huertas and Dr. Piero Lattanzi and the guidance and comments of the Associated Editor, Dr. Josep Soler, have significantly improved the quality of the manuscript. Thanks are given to Cynthia Voelker for the final English review of this manuscript.

REFERENCES

Acero, P., Cama, J., Ayora, C., 2007a. Kinetics of chalcopyrite dissolution at pH 3. European Journal of Mineralogy, 19(2), 173-182.

Acero, P., Cama, J., Ayora, C., 2007b. Sphalerite dissolution kinetics in acidic environment. Applied Geochemistry, 22(9), 1872-1883.

Acero, P., Cama, J., Ayora, C., 2007c. Rate law for galena dissolution in acidic environment. Chemical Geology, 245, 219-229.

Adebayo, A., Ipinmoroti, K., Ajayi, O., 2003. Dissolution kinetics of chalcopyrite with hydrogen peroxide in sulphuric acid medium. Chemical and Biochemical Engineering Quarterly, 17(3), 213-218.

Almodóvar, G., Sáez, R., Pons, J., Maestre, A., Toscano, M., Pascual, E., 1998. Geology and genesis of the Aznalcóllar massive sulphide deposits, Iberian Pyrite Belt, Spain. Mineralum Deposita, 33(1-2), 111-136.

Antonijevic, M., Bogdanovic, G., 2004. Investigation of the leaching of chalcopyritic ore in acidic solutions. Hydrometallurgy, 73(3-4), 245-256.

Antonijevic, M., Jankovic, Z., Dimitrijevic, M., 2004. Kinetics of chalcopyrite dissolution by hydrogen peroxide in sulphuric acid. Hydrometallurgy, 71(3-4), 329-334.

Aydogan, S., Ucar, G., Canbazoglu, M., 2006. Dissolution kinetics of chalcopyrite in acidic potassium dichromate solution. Hydrometallurgy, 81(1), 45-51.

Barrante, J., 1974. Applied Mathematics for Physical Chemistry. Prentice-Hall, New Jersey, Englewood Cliffs, 173 pp.

Biegler, T., Horne, M., 1985. The electrochemistry of surface oxidation of chalcopyrite. Journal of the Electrochemical Society, 132(6), 1363-1369.

Brunauer, S., Emmet, P., Teller, E., 1938. Adsorption of gases in multimolecular layers. Journal of the American Chemical Society, 60, 309-319.

Buckley, A., Woods, R., 1984. An X-Ray Photoelectron Spectroscopy study of the oxidation of chalcopyrite. Australian Journal of Chemistry, 37(12), 2403-2413.

Cama, J., Acero, P., 2005. Dissolution of minor sulphides present in a pyritic sludge at pH 3 and 25ºC. Geologica Acta, 3, 15-26.

Cama, J., Acero, P., Ayora, C., Lobo, A., 2005. Galena surface reactivity at acidic pH and 25 ºC based on flow-through and in situ AFM experiments. Chemical Geology, 214(3-4), 309-330.

Çolak, S., Alkan, M., Kocakerim, M., 1987. Dissolution kinetics of chalcopyrite containing pyrite in water saturated with chlorine. Hydrometallurgy, 18(2), 183-193.

De Giudici, G., Zuddas, P., 2001. In situ investigation of galena dissolution in oxygen saturated solution: Evolution of surface features and kinetic rate. Geochimica et Cosmochimica Acta, 65(9), 1381-1389.

Devi, N., Madhuchhanda, M., Rao, K., Rath, P., Paramguru, R., 2000. Oxidation of chalcopyrite in the presence of manganese dioxide in hydrochloric acid medium. Hydrometallurgy, 57(1), 57-76.

Domènech, C., de Pablo, J., Ayora, C., 2002. Oxidative dissolution of pyritic sludge from the Aznalcóllar mine (SW Spain). Chemical Geology, 190(1-4), 339-353.

Dutrizac, J., 1981. The dissolution of Chalcopyrite in Ferric-Sulfate and Ferric-Chloride Media. Metallurgical Transactions B-Process Metallurgy, 12(2), 371-378.

Dutrizac, J., 1990. Elemental sulfur formation during the ferric-chloride leaching of chalcopyrite. Hydrometallurgy, 23(2-3), 153-176.

Fairthorne, G., Fornasiero, D., Ralston, J., 1997. Effect of oxidation on the collectorless flotation of chalcopyrite. International Journal of Mineral Processing, 49(1-2), 31-48.

Farquhar, M., Wincott, P., Wogelius, R., Vaughan, D., 2003. Electrochemical oxidation of the chalcopyrite surface: an

XPS and AFM study in solution at pH 4. Applied Surface Science, 218(1-4), 34-43.

Hackl, R., Dreisinger, D., Peters, E., King, J., 1995. Passivation of Chalcopyrite during oxidative leaching in sulfate media. Hydrometallurgy, 39(1-3), 25-48.

Harmer, S.L., Thomas, J.E., Fornasiero, D., Gerson, A. R., 2006. The evolution of surface layers formed during chalcopyrite leaching. Geochimica et Cosmochimica Acta, 70(17), 4392-4402.

Hiroyoshi, N., Miki, H., Hirajima, T., Tsunekawa, M., 2000. A model for ferrous-promoted chalcopyrite leaching. Hydrometallurgy, 57(1), 31-38.

Hiroyoshi, N., Miki, H., Hirajima, T., Tsunekawa, M., 2001. Enhancement of chalcopyrite leaching by ferrous ions in acidic ferric sulfate solutions. Hydrometallurgy, 60(3), 185-197.

Holliday, R., Richmond, W., 1990. An electrochemical study of the oxidation of chalcopyrite in acidic solution. Journal of Electroanalytical Chemistry, 288(1-2), 83-98.

Janzen, M., Nicholson, R., Scharer, J., 2000. Pyrrhotite reaction kinetics: Reaction rates for oxidation by oxygen, ferric iron, and for nonoxidative dissolution. Geochimica et Cosmochimica Acta, 64(9), 1511-1522.

Klauber, C., 2003. Fracture-induced reconstruction of a chalcopyrite ($CuFeS_2$) surface. Surface and Interface Analysis, 35(5), 415-428.

Klauber, C., Parker, A., van Bronswijk, W., Watling, H., 2001. Sulphur speciation of leached chalcopyrite surfaces as determined by X-ray photoelectron spectroscopy. International Journal of Mineral Processing, 62(1-4), 65-94.

Lasaga, A., Soler, J., Ganor, J., Burch, T., Nagy, K., 1994. Chemical weathering rate laws and global geochemical cycles. Geochimica et Cosmochimica Acta, 58(10), 2361-2386.

Lochmann, J., Pedlik, M., 1995. Kinetic anomalies of dissolution of sphalerite in ferric sulfate solution. Hydrometallurgy, 37(1), 89-96.

Lu, Z., Jeffrey, M., Lawson, F., 2000. The effect of chloride ions on the dissolution of chalcopyrite in acidic solutions. Hydrometallurgy, 56(2), 189-202.

Mikhlin, Y., Tomashevich, Y., Asanov, I., Okotrub, A., Varnek, V., Vyalikh, D., 2004. Spectroscopic and electrochemical characterization of the surface layers of chalcopyrite ($CuFeS_2$) reacted in acidic solutions. Applied Surface Science, 225(1-4), 395-409.

Munoz, P., Miller, J., Wadsworth, M., 1979. Reaction-mechanism for the acid ferric sulfate leaching of chalcopyrite. Metallurgical Transactions B-Process Metallurgy, 10(2), 149-158.

Nordstrom, D., 2000. Aqueous Redox Chemistry and the Behavior of Iron in Acid Mine Waters. In: Wilkin, R.D., Ford, R. (eds.). Proceedings of the Workshop on Monitoring Oxidation-Reduction Processes for Ground-water Restoration. Enviromental Protection Agency, EPA/600/R-02/002, 43-47.

Palmer, B., Nebo, C., Rau, M., Fuerstenau, M., 1981. Rate phenomena involved in the dissolution of chalcopyrite in chloride-bearing lixiviants. Metallurgical Transactions B-Process Metallurgy, 12(3), 595-601.

Parker, A., Paul, R., Power, G., 1981. Electrochemistry of the oxidative leaching of copper from chalcopyrite. Journal of Electroanalytical Chemistry, 118(FEB), 305-316.

Parkhurst, D., 1995. User's guide to PHREEQC: A computer program for speciation, reaction path, advective-transport, and inverse geochemical calculations. U.S. Geological Survey, Water-Resources Investigations Report 95-4227, 143 pp.

Price, D., Warren, G., 1986. The influence of silver ion on the electrochemical response of chalcopyrite and other sulfide electrodes in sulfuric-acid. Hydrometallurgy, 15(3), 303-324.

Rimstidt, J., Chermak, J., Gagen, P., 1994. Rates of reaction of galena, sphalerite, chalcopyrite and arsenopyrite with Fe(III) in acidic solutions. In: Alpers, C.N., Blowes, D.W. (eds.). Environmental geochemistry of sulfide oxidation. American Chemical Symposium, Series 550, Washington DC, 2-13.

Rosso, K., Vaughan, D.J., 2006. Reactivity of Sulfide Mineral Surfaces. In: Vaughan, D.J. (ed.). Sulfide Mineralogy and Geochemistry. Reviews in Mineralogy and Geochemistry (61), Mineralogical Society of America, Chantilly, Virginia, 557-607.

Salmon, S.U., Malmström, M.E., 2006. Quantification of mineral dissolution rates and applicability of rate laws: Laboratory studies of mill tailings. Applied Geochemistry, 21(2), 269-288.

Scharer, J., Nicholson, R., Halbert, B., Snodgrass, W., 1994. A computer program to assess acid generation in pyritic tailings. In: Alpers, C.N., Blowes, D.W. (eds.). Environmental geochemistry of sulfide oxidation. American Chemical Symposium Series 550, Washington DC, 132-152.

Todd, E., Sherman, D., Purton, J., 2003. Surface oxidation of chalcopyrite ($CuFeS_2$) under ambient atmospheric and aqueous (pH 2-10) conditions: Cu, Fe L- and OK-edge X-ray spectroscopy. Geochimica et Cosmochimica Acta, 67(12), 2137-2146.

Velásquez, P., Leinen, D., Pascual, J., Ramos-Barrado, J. R., Grez, P., Gómez, H., Schrebler, R., Del Río, R., Córdova, R., 2005. A chemical, morphological, and electrochemical (XPS, SEM/EDX, CV, and EIS) analysis of electrochemically modified electrode surfaces of natural chalcopyrite ($CuFeS_2$) and pyrite (FeS_2) in alkaline solutions. Journal of Physical Chemistry B, 109(11), 4977-4988.

Weisener, C., Smart, R., Gerson, A., 2003. Kinetics and mechanisms of the leaching of low Fe sphalerite. Geochimica et Cosmochimica Acta, 67(5), 823-830.

Weisener, C., Smart, R., Gerson, A., 2004. A comparison of the kinetics and mechanism of acid leaching of sphalerite containing low and high concentrations of iron. International Journal of Mineral Processing, 74(1-4), 239-249.

Manuscript received May 2008;
revision accepted September 2008;
published Online June 2009.